

Energy Autonomous Two-Way Repeater System for Non-Line-of-Sight Interrogation in Next Generation Wireless Sensor Networks

Ajibayo O. Adeyeye¹, Graduate Student Member, IEEE, Charles Lynch², Graduate Student Member, IEEE, Aline Eid³, Graduate Student Member, IEEE, Jimmy G. D. Hester⁴, Member, IEEE, and Manos M. Tentzeris⁵, Fellow, IEEE

Abstract—In this effort, we present a fully energy autonomous two-way repeater system for use in nonline-of-sight (NLOS) interrogation of wireless sensor networks. The proposed system is based on a pair of tunnel diode reflection amplifiers, taking advantage of the existence of a negative differential resistance region that exists when the device is biased at a low voltage in the quantum tunneling region. This enables the development of an ultralow-cost, ultralow-power means to provide amplification. The proposed system demonstrates an ability to extend the total read range of semipassive radio frequency identification (RFID) tags by 4.55 times while consuming over 1000 times less power than comparable technologies, a notable improvement on previously published work. The system shows an ability to be customized to fit a wide array of different applications where NLOS interrogation and the read range of semipassive RFID tags pose a challenge.

Index Terms—Backscattering, Internet of Things (IoT), negative differential resistance, radio frequency identification (RFID), repeaters, tunnel diode.

I. INTRODUCTION

THE proliferation of the Internet of Things (IoT) and wireless sensor networks (WSNs) over the last few decades has ensured the continued pursuit of new technologies and technological advancements that make the desired ubiquity of the IoTs and WSNs more feasible. One such technology that has seen increasing development and practical applications particularly in radio frequency identification (RFID) systems is modulated backscatter.

Modulated backscatter presents a unique, high energy efficiency communication scheme whereby a radio frequency (RF) tag does not locally generate an RF signal for

communications. Instead, an interrogating antenna illuminates the tag and it is able to reflect the incident signal with a coefficient of reflection that varies with the load seen by the terminals of the antenna. Typically, the tag is comprised of a single antenna and switch front end to enable the load modulation. The high energy efficiency of this scheme makes it very suitable for dense and networked implementations as the communicating devices/sensor nodes can then be made energy autonomous and operated without need of batteries or other constant sources of energy.

Despite this high energy efficiency, backscatter in RFID implementations suffers from severe limitations in the read range. This comes as a direct result of the aforementioned benefit of the modulated backscatter scheme where no RF signal is generated at the tag. Hence, the power received by the interrogating antenna decays to the fourth power of the distance between the reader and the tag. This effect is even more evident at frequencies higher than the traditional ultrahigh-frequency (UHF) implementations that exist in the 300-MHz–3-GHz range. Higher frequencies at 5.8 GHz and even up to 24 and 60 GHz have gained traction for use in the IoTs and WSNs because of their much smaller form factors [1]–[3]. However, this reduced form factor comes at a price and the already expensive link budget becomes even more so as the effective aperture area of the antenna decreases with increasing frequency.

A variety of approaches to increase the range of modulated backscatter RFID have been proposed in the literature. The use of a carrier emitter in a bistatic configuration is proposed in [4] and [5] where a series of devices detached from the reader is used to synthesize a carrier signal and placed closer to the RFID tags to improve the link budget; however, in the latter effort, the achievable range is limited by the emitter power output, and in the former effort, the power consumption of each carrier emitter tends toward tens of milliwatts depending on the desired output power and application. Repeater nodes are proposed in [6]–[10] and these generally work well and pose an effective solution for passive RFID systems; however, a major limitation is the power consumption of the repeater nodes, which is driven up by the use of amplifiers.

Reflection amplifiers have been integrated into tag architectures in order to enable long-range detection in [1] and [11]–[13]. These methods, however, do not scale very well for dense implementations due to increased costs asso-

Manuscript received October 19, 2021; accepted November 30, 2021. Date of publication February 1, 2022; date of current version March 4, 2022. This work was supported in part by the Georgia Research Alliance under Grant 10.13039/100008065, in part by the Air Force Research Laboratory under Grant 10.13039/100006602, and in part by Florida International University under Grant 10.13039/100007681. This article is an expanded version from the International Microwave Symposium, Atlanta, June 8 2021 [DOI: 10.1109/LMWC.2021.3064734]. (Corresponding author: Ajibayo O. Adeyeye.)

Ajibayo O. Adeyeye, Charles Lynch, and Manos M. Tentzeris are with the Department of Electrical and Computer Engineering, Georgia Institute of Technology, Atlanta, GA 30332 USA (e-mail: aadeyeye3@gatech.edu).

Aline Eid is with the Massachusetts Institute of Technology, Cambridge, MA 02139 USA.

Jimmy G. D. Hester is with Atheraxon, Inc., Atlanta, GA 30308 USA.

Color versions of one or more figures in this article are available at <https://doi.org/10.1109/TMTT.2022.3144320>.

Digital Object Identifier 10.1109/TMTT.2022.3144320

ciated with the active device attached to every tag in its implementation. Repeaters prove to be a particularly attractive option for use in range extension for the following reasons.

- 1) Repeaters are easily compatible with legacy systems and can be designed and used in a plug-and-play fashion for existing RFID systems at the desired frequency.
- 2) Low cost of implementation as the repeater architecture is generally made up of two components: the amplifying element and the radiating element.
- 3) Two-way repeaters can be used to extend coverage in nonline-of-sight (NLOS) scenarios where a reader does not have a direct path to a tag of interest.

In this article, we expand upon a previously published work in [14]. Here, a 4.5 times improvement in the read range is reported in comparison with the two times increase in the previous effort. In addition to a more in-depth technical and mathematical analysis of the proposed system's capabilities and limitations, a fully energy autonomous repeater is demonstrated in an indoor sensing application to show a real-world application of the proposed device.

The rest of this article is organized as follows. Section II presents an in-depth discussion of the proposed repeater architecture, specifically highlighting the tunnel diode-based reflection amplifier as well as a full characterization of the device. Next, a detailed link budget analysis of the two-way repeater is carried out in Section III. Section IV presents the measurement results characterizing the tag repeater and reader to repeater links by observing the achievable signal-to-noise ratio at different distances as well as presenting a characterization of the amplification bandwidth of the channel. Section V presents an energy autonomous operation of the repeater node with a photo-sensing application. Concluding remarks and direction for future work are given in Section VI.

II. REPEATER ARCHITECTURE

The repeater system proposed in this work is made up of a pair of tunnel diode-based reflection amplifiers that are used to overcome limitations imposed on the link budget of a backscatter RFID system operating in the 5.8-GHz industrial, scientific, and medical (ISM) band. This proves especially useful in situations where there is no available line-of-sight path between a displaced reader and a set of tags as shown in Fig. 1. The repeater is designed to operate such that both the interrogating signal in the uplink and the received signal from the tag in the downlink are amplified. In the majority of current applications of the two-way repeater architecture, a major concern is the level of isolation achievable between the devices responsible for amplifying the signal in the reader-to-tag link and the tag-to-reader link. The isolation between the respective devices must be greater than the resultant amplification; otherwise, the ensuing positive feedback would saturate the amplifying devices. Thus, for two-way repeater architectures where isolation cannot be accomplished by decoupling the two devices electromagnetically either via physical separation or some other means, complicated adaptive cancellation circuits and techniques must be deployed, which invariably increases drastically the associated monetary costs and power consumption associated with the deployment of such a system. In our proposed system, the devices are designed such that there is

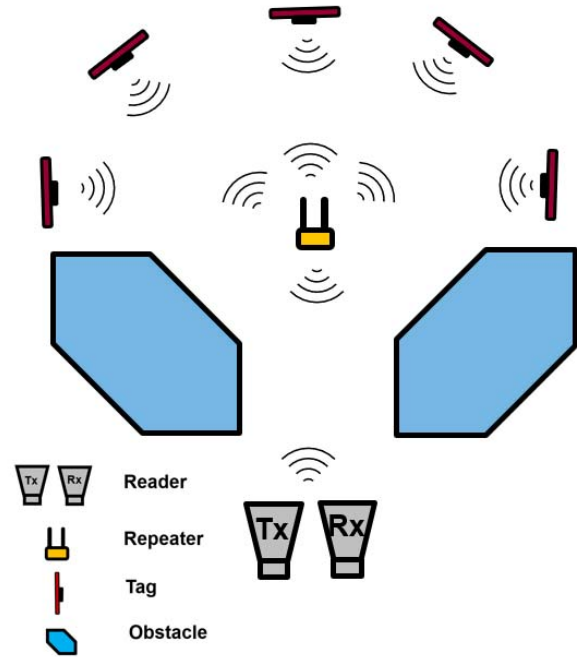


Fig. 1. Proposed repeater architecture in the NLOS case of a single bistatic reader (colocated TX/RX), multiple tags and repeater.

a small difference in the operating frequency. As a result, the interrogating signal from the reader and the modulated backscatter return from the tag are amplified in two distinct channels separated in frequency in a low-cost architecture.

A. Tunnel Diode-Based Reflection Amplifier

Whenever some antenna is terminated with a particular load and some interrogating signal is incident on the structure, a signal is reflected with a reflection coefficient, Γ . The complex-valued reflection coefficient describes how the incident signal is changed due to the observed change in impedance as the signal propagates from the antenna to the connected load. The magnitude of the reflection coefficient, $|\Gamma|$ given in (1), indicates how the amplitude of the signal is changed and is bound such that $0 < |\Gamma| < 1$, indicating that either all of the incident signal is reflected when the load impedance $Z_L = 0$ or none of the signal is reflected when the antenna impedance $Z_A = Z_L$

$$|\Gamma| = \left| \frac{Z_L - Z_A^*}{Z_L + Z_A^*} \right|. \quad (1)$$

A reflection amplifier is able to break this constraint on the magnitude of the reflection coefficient looking into a terminated antenna. It is able to accomplish this by presenting a negative input impedance at the terminals of the antenna, so from (1), it is evident that when $Z_L < 0$, then $|\Gamma| > 1$, which results in the incident signal being amplified in reflection by a factor equal to the magnitude of the resultant reflection coefficient. This can be accomplished using various active devices such as the field-effect transistor (FET),

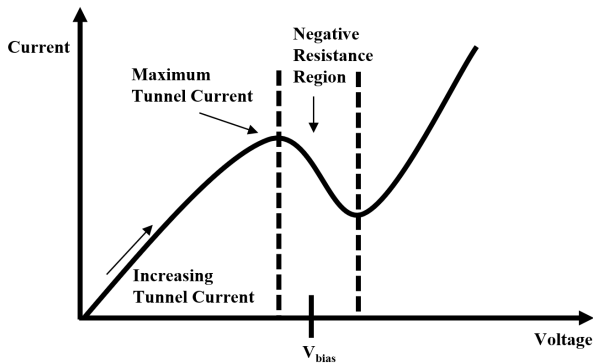


Fig. 2. I - V characteristics of tunnel diode.

bipolar junction transistor (BJT), or some other metal–oxide–semiconductors that, under some biasing condition, are able to provide the desired amplification. Reflection amplifiers have seen use in a wide range of RFID applications. Notably, they have been included as part of the tag front end in semipassive RFID deployments [11]. Another class of active devices that has been proposed in the literature for use in reflection amplifiers is the tunnel diode.

The tunnel diode is a two-terminal semiconductor device that is heavily overdoped with impurities so that the depletion region is much narrower than that of a conventional p-n-junction diode. This extremely narrow depletion region means that only a very small amount of voltage is needed to produce current through the tunnel diode. As a result of the heavy doping, some electrons in the conduction band of the n-type semiconductor and some holes in the valence band of the p-type semiconductor are at the same Fermi energy level. Therefore, at very small bias voltages, electrons are able to tunnel from the conduction band to the valence band causing a small current to flow. As this voltage is increased, the tunneling current increases up to a certain point where the energy level in the conduction and valence bands is equal in which case the maximum tunneling current is achieved. When the voltage is increased further, there is an increasing difference in the energy levels in the conduction and valence bands, so the tunneling current starts to decrease, which presents a negative differential region at this bias voltage. Increasing the applied voltage even further, the conduction and valence bands no longer have any overlap and the tunnel diode begins operating as a regular p-n-junction diode [15], [16]. This effect is summarized by the labeled I - V characteristic curve in Fig. 2.

What makes the tunnel diode so attractive for use as the active element in a reflection amplifier is the fact that the negative resistance region occurs at a very low input bias voltage; much less than that required for FETs, BJTs, or other CMOS devices considered for use. Typically, bias voltages less than 200 mV are needed to operate the tunnel diode in this region.

B. Design, Fabrication, and Characterization of Tunnel Diode Reflection Amplifier

The reflection amplifier used in this effort was adapted from the design presented in [13]. The device features the MBD2057 tunnel diode, a transmission-line-based matching

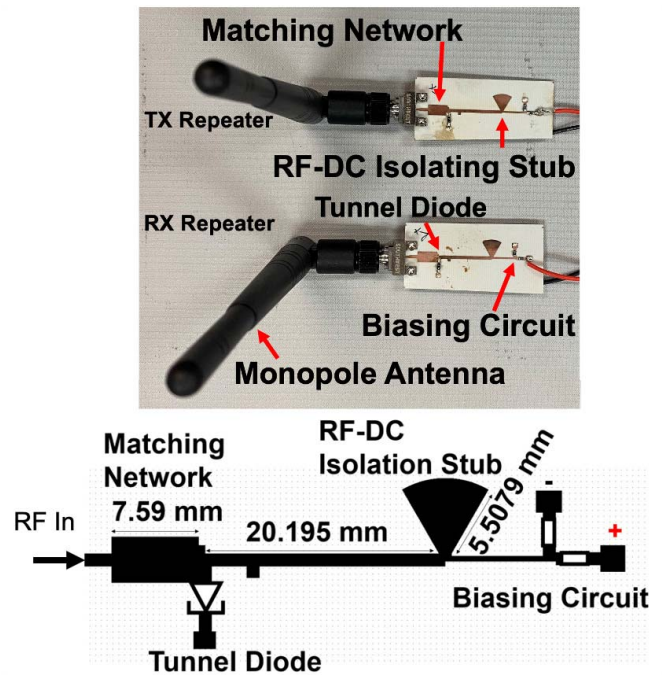


Fig. 3. Designed and fabricated reflection amplifier.

network, tuning stub, and an RF-to-dc isolation stub, as shown in Fig. 3.

The reflection amplifier circuit was fabricated on the Rogers RO4350b substrate featuring permittivity $\epsilon_r = 3.48$ and loss tangent $\tan \delta = 0.0037$ and a thickness of 0.51 mm. The fabrication process involved an inkjet masking procedure where Microchem SU8 was inkjet printed onto the copper-clad surface of the substrate using the Dimatix DMP-2850 printer. The SU8 acts like a positive photoresist, so the sections of the copper surface not covered by SU8 are etched away using an iron chloride solution.

After fabrication, the next step was characterization of the tunnel diode reflection amplifier. As is typical for conventional amplifiers, we are most interested in the gain performance as well as the frequency response of the reflection amplifier in response to changes in the bias voltage. The amplifier was characterized via a two-port network analyzer measurement. Necessary for use in the characterization measurement was a three-port circulator. The circulator is a passive device that only allows RF energy incident at any of its ports to exit at the port immediately following it in a particular direction. Therefore, a signal entering at port 1 exits at port 2, a signal entering at port 2 exits at port 3, and a signal entering at port 3 exits at port 1. The circulator in use for these measurements was the PE8402 featuring 18-dB isolation and a maximum insertion loss of 0.5 dB. In the measurement setup, port 1 of the circulator was fed with an RF signal from the network analyzer, the reflection amplifier being characterized was placed at port 2, and port 3 was connected to the second port on the network analyzer to observe the amplified signal, as shown in Fig. 4. Tunnel diode-based reflection amplifiers have been reported to show a linear relationship between the chosen bias voltage and the peak operating frequency [5], [12]. The fabricated reflection amplifier was biased with voltages

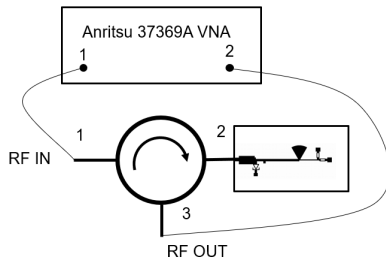


Fig. 4. Reflection amplifier characterization setup.

ranging from 100 to 200 mV for a fixed input power of -60 dBm in order to find the frequency of operation that provides an adequate level of gain and also exists in the desired frequency band. The results of this measurement are shown in Fig. 5(a). It is also indicated that there is a range of bias voltages and corresponding operating frequencies for which the realizable gain of the amplifier is above 35 dB. This very much fits the purpose and design of the proposed system because the reflection amplifiers used in the uplink and downlink can be tuned to different frequencies of operation in our band of interest; then, the only limitation becomes the chosen modulation frequencies for the RFID tags being interrogated, as shown in Fig. 5. Tunnel diodes are known to experience variability in performance across different manufactured devices, with each manufactured device exhibiting a potentially different quantum tunneling region. This shows up as differences in the operating frequency and necessary bias voltage of the fabricated reflection amplifier.

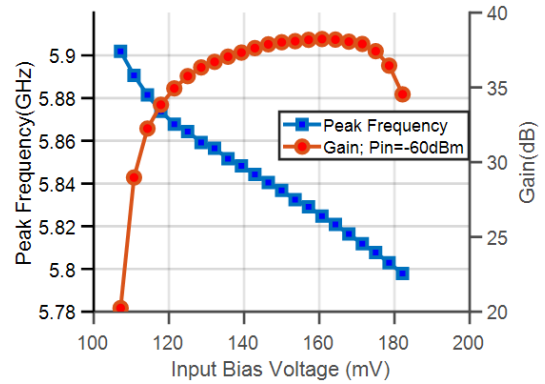
Once a particular bias voltage was chosen, the amplifier gain for a range of input powers from -30 to -90 dBm was characterized with the results shown in Fig. 6. The results show that for the chosen bias voltage, gain up to 50 dB at input power less than -90 dBm was achievable. Observed also in the measurements is a reduction in the gain as the input power was increased, and this is due to the saturation of the tunnel diode at increased levels of incident power.

III. LINK BUDGET ANALYSIS

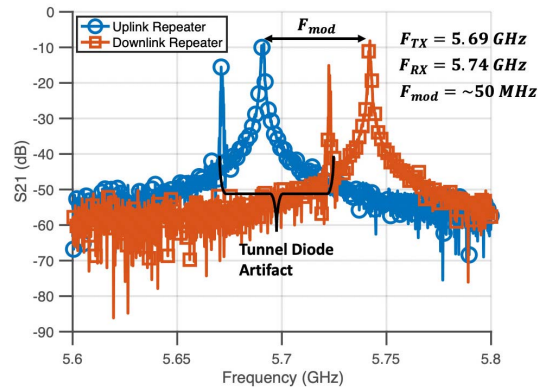
This section goes over a link budget analysis for the proposed repeater system in order to observe its benefits. To derive the received power at the receiver, propagation in the four different paths of the link must be considered. They are given as follows:

- 1) reader to uplink repeater;
- 2) uplink repeater to tag;
- 3) tag to downlink repeater;
- 4) downlink repeater to reader.

These propagation paths were analyzed starting from the well-known Friis free-space propagation equation, which is given in decibel scale by (2) where P_r is the received power in dBm, P_t is the transmit power in dBm, G_t and G_r are the gains of the transmitting and receiving antennas, respectively, in dBi, λ is the wavelength in free space, n is the path loss exponent, and d is the distance between the transmitter and the designated receiver. Although propagation in RFID systems is two-way, for the purpose of this analysis, we consider



(a)



(b)

Fig. 5. Reflection amplifier characterization. (a) Peak frequency versus input bias voltage and gain versus input bias voltage. (b) Uplink/downlink repeater characterization.

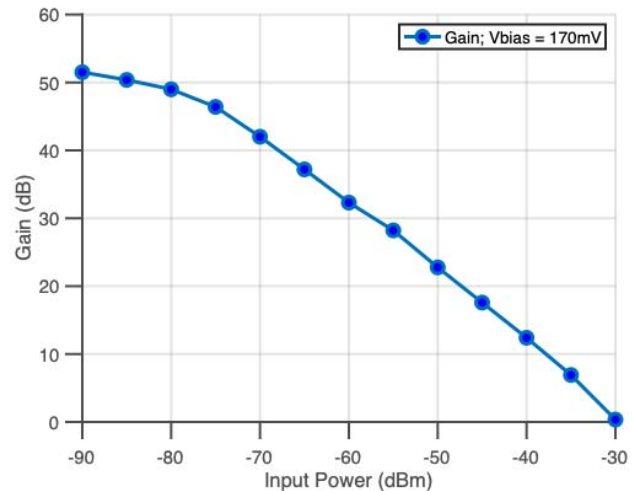


Fig. 6. Measured reflection amplifier gain versus input power.

a one-way link budget for the four different paths to get ultimately the power of the subcarrier received at the reader. A schematic representation is shown in Fig. 7

$$P_r = P_t + G_t + G_r + 10n \log_{10} \left(\frac{\lambda}{4\pi d} \right). \quad (2)$$

1) Reader to Uplink Repeater:

$$P_{r,rp}^{rx} = P_{r,rp}^{tx} + G_r^{rx} + G_{rp}^{tx} + 10n \log_{10} \left(\frac{\lambda}{4\pi d_{r,rp}} \right) \quad (3)$$

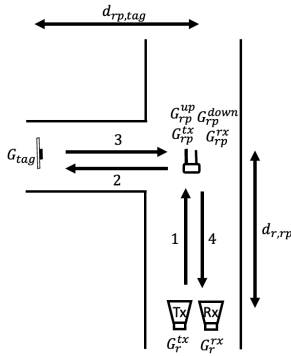


Fig. 7. Propagation path for link budget analysis.

$$P_{rp,tag}^{tx} = P_{r,rp}^{rx} + G_{rp}^{up}. \quad (4)$$

2) *Uplink Repeater to Tag:*

$$P_{rp,tag}^{rx} = P_{rp,tag}^{tx} + G_r^{tx} + G_{tag} + 10n \log_{10} \left(\frac{\lambda}{4\pi d_{rp,tag}} \right) \quad (5)$$

$$P_{tag,rp}^{tx} = P_{rp,tag}^{rx} + M. \quad (6)$$

3) *Tag to Downlink Repeater:*

$$P_{tag,rp}^{rx} = P_{tag,rp}^{tx} + G_{tag} + G_{rp}^{rx} + 10n \log_{10} \left(\frac{\lambda}{4\pi d_{rp,tag}} \right) \quad (7)$$

$$P_{rp,r}^{tx} = P_{tag,rp}^{rx} + G_{rp}^{down}. \quad (8)$$

4) *Downlink Repeater to Reader:*

$$P_r^{rx} = P_{rp,r}^{tx} + G_{rp}^{rx} + G_r^{rx} + 10n \log_{10} \left(\frac{\lambda}{4\pi d_{r,rp}} \right). \quad (9)$$

Here, parameters are listed as follows.

- 1) $P_{r,rp}^{rx}$ is the power received by the uplink repeater from the reader (dBm).
- 2) $P_{r,rp}^{tx}$ is the power transmitted by the reader to the repeater (dBm).
- 3) G_r^{tx} is the gain of the reader transmit antenna (dBi).
- 4) G_{rp}^{tx} is the gain of the repeater uplink antenna (dBi).
- 5) $d_{r,rp}$ is the distance between the reader and the repeater (m).
- 6) $P_{rp,tag}^{tx}$ is the power transmitted from the repeater to the tag (dBm).
- 7) G_{rp}^{up} is the gain of the uplink reflection amplifier (dB).
- 8) $P_{rp,tag}^{rx}$ is the power received by the tag from the uplink repeater (dBm).
- 9) G_{tag} is the gain of the RFID tag antenna (dBi).
- 10) $d_{rp,tag}$ is the distance between the repeater and the tag (m).
- 11) $P_{tag,rp}^{tx}$ is the power transmitted from the tag to the downlink repeater (dBm).
- 12) M is the modulation factor of the RFID tag (dB).
- 13) $P_{tag,rp}^{rx}$ is the power received by the downlink repeater from the tag (dBm).
- 14) G_{rp}^{rx} is the gain of the downlink repeater antenna (dBi).
- 15) $P_{rp,r}^{tx}$ is the power transmitted from the downlink repeater to the reader.
- 16) G_{rp}^{down} is the gain of the downlink reflection amplifier (dB).

17) G_r^{rx} is the gain of the reader antenna (dBi).

18) P_r^{rx} is the power received by the reader from the downlink repeater.

The above equations and listed parameters describe a simple model for the link budget of the two-way repeater system. For simplicity, no additional losses are included in the model and an ideal backscattering RFID tag is modeled with $M = -3$ dB. The antenna gains $G_r^{tx} = G_r^{rx} = 9$ dBi; 5.8-GHz monopole antennas are chosen for the repeater and tag antennas, so $G_{rp}^{tx} = G_{rp}^{rx} = G_{tag} = 1.5$ dBi. A path loss exponent of $n = 1.5$ is chosen for the analysis due to the nature of the environment of the measurement setup and use of directive horn antennas to illuminate the repeater system. In the hallways where the measurements were carried out, the dominant component of the interrogation came from the line-of-sight path to the reader. The gain of the reflection amplifier was characterized for a range of input powers up to the saturation point at -30 dBm. A polynomial fit was then used to interpolate the data from Fig. 6. It was assumed that the resultant polynomial function was identical for the uplink and downlink amplifiers and also that the maximum gain achievable was 49.52 dB that was the gain realized at -90 -dBm input power. For input powers below the saturation point, the gain was assumed to be 0 dB. The consequence of using this function for the gain is that in this analysis, the gain of the reflection amplifiers now become functions of the power output from the reader, the distance between the tag and the repeater, and the distance between the reader and the repeater. To find out coverage, the important quantity is the achievable signal-to-noise ratio given a particular reader sensitivity. In this analysis, the sensitivity is assumed to be -130 dBm; however, in real-world implementations, much lower sampling rates could be realized and better TX/RX coupling achieved in order to enable higher receiver sensitivity, which would invariably increase the coverage.

The outlined equations are synthesized in MATLAB to evaluate the coverage benefits of including the repeater as part of the interrogation system of a semipassive RFID tag. The coverage region for successful tag interrogation is defined by the condition: $SNR \geq 5$ dB.

The two distances, $d_{rp,tag}$ and $d_{r,rp}$, were swept in the simulation and the equivalent isotropic radiated power (EIRP) was held constant at 0, 17, and 36 dBm. With 36 dBm being the maximum allowable EIRP in the 5.8-GHz frequency band. The coverage map result for the resulting three conditions is shown in Fig. 8(a)–(c), each on a logarithmic distance scale.

As expected, with increasing EIRP, there is an increase in the total coverage area. However, unlike in the 0-dBm case, for the 17- and 36-dBm scenarios, there is an additional increase in coverage that occurs at the reader-to-repeater distances of 7 and 120 m, respectively. This shows up as inflections at those distances in Fig. 8(b) and (c). The inflection occurs as a result of the tunnel diode reflection amplifier being in saturation until its input power is less than -30 dBm. For all of the input powers greater than the saturation point, the gain is simulated to be 0 dB. The inflection point is where the input power to the forward link repeater is first less than -30 dBm. This is confirmed in Fig. 9, which shows the gain profile of the uplink

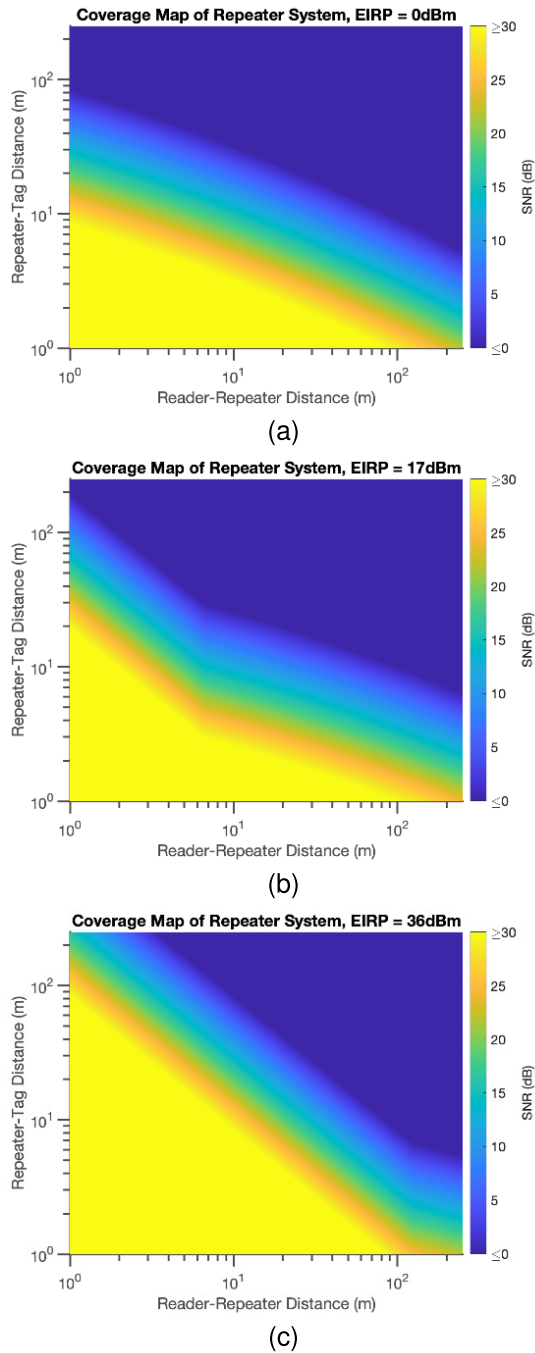


Fig. 8. Repeater link budget analysis coverage map. (a) EIRP = 0 dBm. (b) EIRP = 17 dBm. (c) EIRP = 36 dBm.

repeater over the reader-to-repeater distance for the different EIRP conditions.

This framework presents a systematic way for the repeater system to be designed and deployed to fit a variety of custom applications. For example, for shorter range extension and coverage requirements, a lower EIRP may be utilized as this would drive down the power consumption costs of the signal transmission. The results also show remarkable improvement in the RFID coverage across a wide range of distances when compared with the coverage map for a system with a 0-dB gain repeater, as shown in Fig. 10. The 0-dB gain repeater system is used to model a conventional RFID link without a

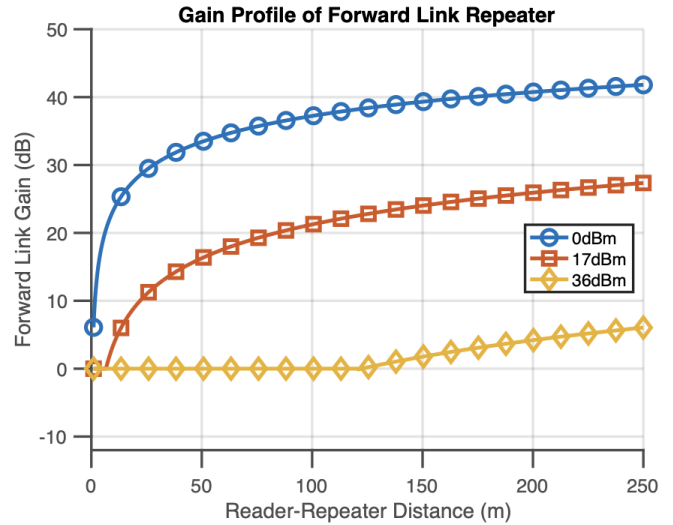


Fig. 9. Simulated gain profile for the forward link repeater.

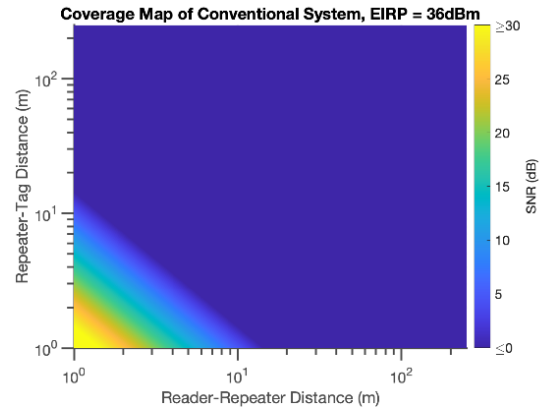


Fig. 10. Coverage map for conventional system with a 0-dB gain repeater. repeater present but preserving the NLOS configuration used to evaluate the proposed system.

IV. MEASUREMENTS

The results of the preceding link budget analysis were verified via measurement in a real-world scenario. To properly evaluate the proposed system, a 5.8-GHz semipassive RFID tag was interrogated by itself and used to set a baseline for the performance and coverage benefits of using the repeaters. This was done by continuously displacing the tag in front of the reader setup until a consistent signal-to-noise ratio of about 10 dB was observed. This condition occurred at a distance of 18 m with 36 dBm of EIRP. The reader setup consisted of a pair of 9-dBi gain horn antennas to transmit and receive, the NI USRP N210 software-defined radio (SDR) to synthesize the interrogating signal, and the Tektronix RSA 4308A spectrum analyzer to observe the received subcarrier. The SKY66288-11 power amplifier featuring 28-dB gain was included in the TX link since the output of the USRP is limited to only 8 dBm. The GVA-8+ gain block featuring 12-dB gain was included in the RX chain to improve sensitivity.

A. Repeater-to-Tag Link Characterization

In this link characterization, the repeater was placed at the corner of a hallway in an office building. The reader setup was

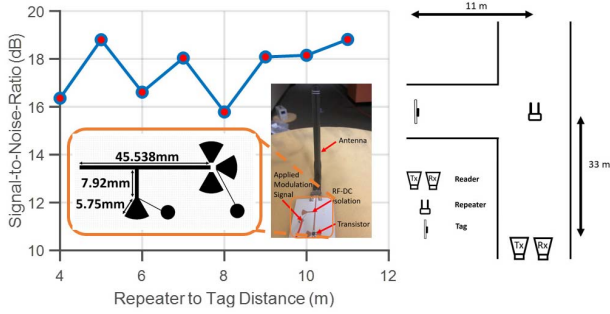


Fig. 11. Measured SNR variation over tag-repeater distance.

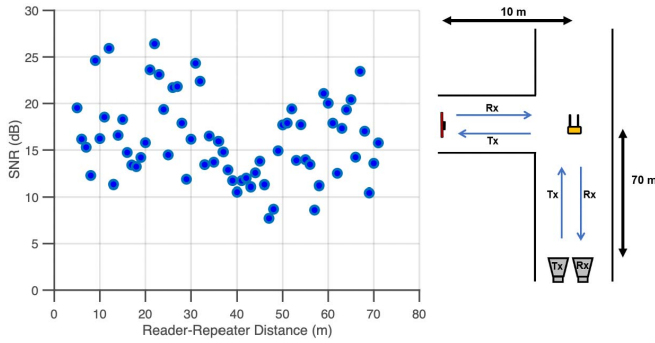


Fig. 12. Measured SNR variation over reader-to-repeater distance.

set at a distance of 33 m from the repeater and the tag was moved in 1-m steps from 4 to 11 m away from the repeater and around the corner from the reader setup. The EIRP for this measurement scenario was set to 17 dBm and the spectrum analyzer sampling rate was at 200 kHz. The signal-to-noise ratio of the subcarrier in the returned spectrum is shown in Fig. 11. It is shown that for the set EIRP, the signal-to-noise ratio stays relatively constant as the tag-to-repeater distance is increased. Intuitively, it would be expected to observe the degradation of the SNR with increasing repeater-to-tag distance. However, the effects of the wireless propagation environment heavily influence the received power at the reader and invariably the SNR. The NLOS link is able to be extended to a total of 44 m, which corresponds to a range extension of 2.44 times as previously reported in [14].

B. Reader-to-Repeater Link Characterization

With the repeater fixed in location, the other link to be characterized is the reader-to-repeater link. In this characterization, however, the tag is fixed at a distance of 10 m from the repeater and the reader setup is stepped between a distance of 5 and 71 m in steps of 1 m. The average of five successive spectrum analyzer measurements was taken for each discrete distance measured. Across this range with the EIRP fixed at 36 dBm, a signal-to-noise ratio of at least 10 dB is obtained for the majority of the distances. There is an expected downtrend in the signal-to-noise ratio as the reader-to-repeater link is stretched, which is expected for a constant EIRP as shown in Fig. 12. Small- and large-scale fading properties of the wireless channel through which the signal propagates also play a role in the variation of the

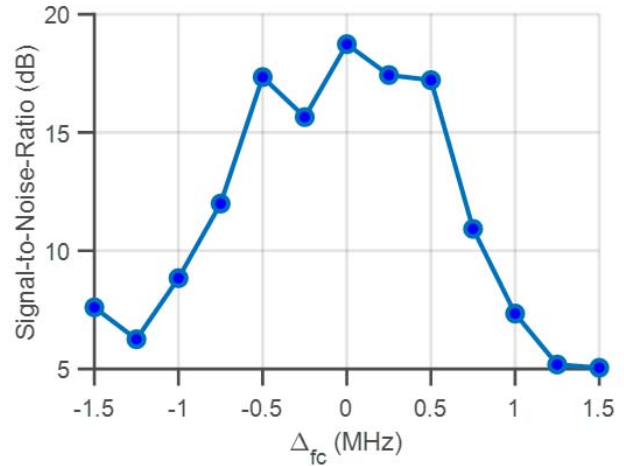


Fig. 13. Amplification bandwidth.

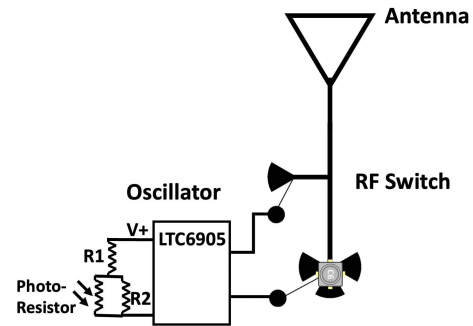


Fig. 14. RFID-based light sensor architecture.

SNR obtained at the reader. This link characterization shows a total coverage distance up to 82 m corresponding to a range extension of 4.55 times and a marked improvement upon the 2.44 times reported prior. These measurements in combination with the simulation results presented in Fig. 9 suggest that even more extreme range extension can be realized.

C. Channel Amplification Bandwidth Characterization

It is also important to have an understanding of the range of frequencies that can be amplified using this system instantaneously. To do this, the tag is fixed at a distance of 10 m from the repeater and the reader is fixed at a distance of 30 m from the repeater to be at about the midpoint of the full available range in the measurement environment. The tag and reader maintain no line of sight as in the previous measurements. The carrier frequency of the interrogating signal is changed in steps of 0.25 MHz and the SNR of the returned subcarrier is observed. The results of this measurement are summarized in Fig. 13. With the desired SNR set to be ≥ 5 dB, the instantaneous bandwidth can be seen to be about 3 MHz. This result combined with the ability of the tunnel diode reflection amplifier's operating center frequency to be tuned based on the applied bias voltage opens the door to applications with dynamic tunable repeaters serving a multitude of communicating sensor nodes.

V. ENERGY AUTONOMOUS REPEATER APPLICATION

In order to fully demonstrate the capabilities of the proposed ultralow-power NLOS repeater system, a demonstration of

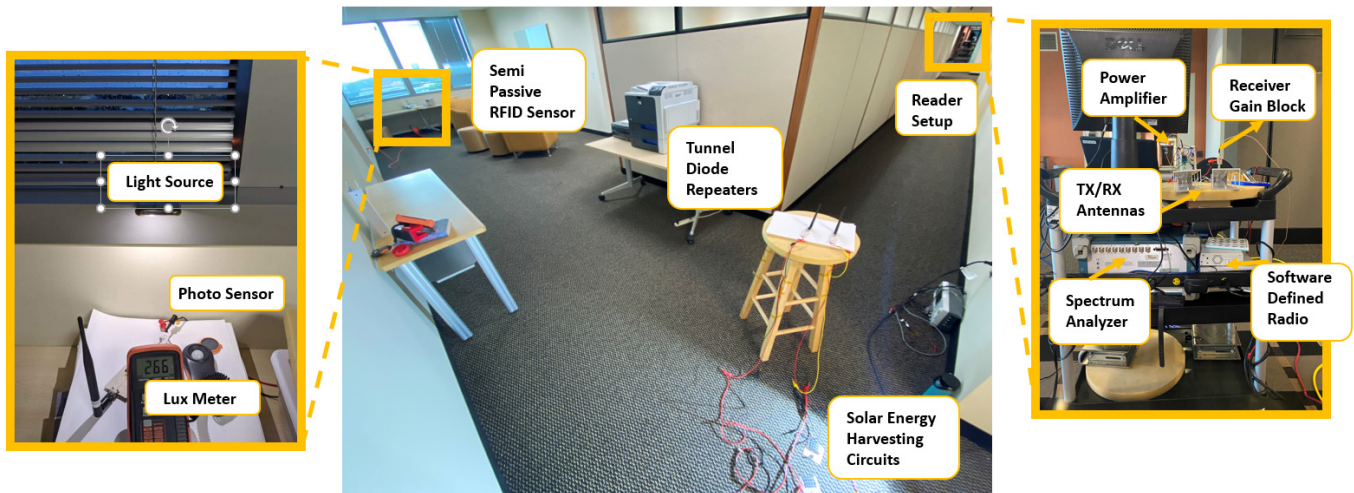


Fig. 15. Interrogation setup for energy autonomous tunnel diode repeater system.

a smart infrastructure application was conducted with the repeater components being completely energy autonomous. The repeater components were powered through the use of a solar cell energy-harvesting circuit. The circuit consisted of a flexible solar cell, an LT3009 adjustable low-power voltage regulator, the required surface mount device (SMD) resistors to produce an output of 1 V, and a 10-k Ω tuning potentiometer in order to operate in the amplifying region of the tunnel diode. The reader setup for this measurement consisted of largely the same components as the previous measurements, but with the NI USRP N210 SDR as the transmitter and receiver to provide a more portable low-cost reader. For this measurement, the interrogator EIRP was set to 36 dBm with a receiver channel sampling rate of 600 kHz. The same semipassive RFID tag used to evaluate the repeater system in the previous measurements was customized, as shown in Fig. 14.

The sensor node is based on the LT6905 oscillator and a photocell. The resistor $R1$ sets the modulation frequency for the RFID tag, while resistor $R2$ is connected in parallel with the photocell in order to control its dynamic range and ensure that the change in resistance due to photosensitivity does not fall outside the range accepted by the LT6905. The sensor node is designed such that the fully bright and fully dark lighting conditions exist within only a few tens of kilohertz of deviation from the initial $R1$ set modulation frequency. The off-the-shelf component selected for the resistive sensing element was a photoresistor, which could be used for smart lighting and energy management applications. This proof-of-concept RFID sensor node architecture could easily be extended to a variety of sensors, including ultralow-cost additively manufactured inkjet-printed chemiresistive or capacitive sensors. Hester and Tentzeris [17] demonstrated the use of chemiresistive ammonia sensor integrated with a long-range backscattering system. The measurement setup of the fully energy autonomous RFID repeater system is shown in Fig. 15.

The measurement consisted of varying the lighting conditions in the vicinity of the sensing node with four different lighting states, thereby increasing the modulation

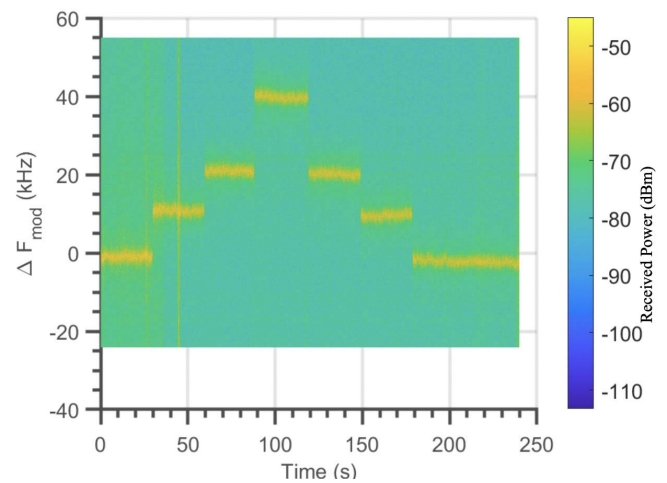


Fig. 16. Short-time Fourier transform of received signal of energy autonomous RFID repeater system NLOS measurement with proof-of-concept sensing node.

frequency of the sensor node. The local lighting intensity was simultaneously measured with a digital luxmeter at each state. A short-time Fourier transform process was applied on the time-domain signal recorded by the SDR. The process involved performing the well-known fast Fourier transform on windowed sections of the time-domain signal and then observing the change in the subcarrier to see the sensor response. The measured received spectrum over time was obtained for the entire 4-min measurement and is shown in Fig. 16. A linear fit of the modulation frequency deviation from ambient lighting conditions was done from these measured states with the estimated sensor node sensitivity to be 5.05 lm/cm²/kHz and is shown in Fig. 17.

This measurement demonstrates the ability of the proposed energy autonomous NLOS RFID repeater system to provide ubiquitous sensing for future data driven in the IoT systems, including applications in smart city and smart agriculture scenarios.

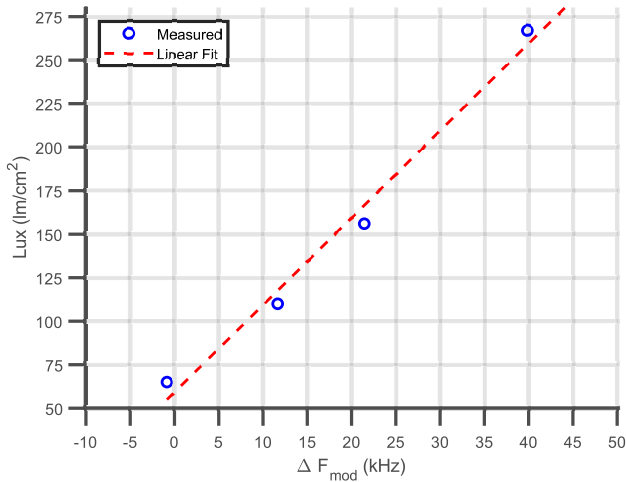


Fig. 17. Linear fit of modulation frequency deviation from ambient lighting conditions versus lux.

TABLE I
REPEATER POWER CONSUMPTION COMPARISON

	Power Consumption	Operating Band	Voltage	Gain
This work	40 μ W	5.8 GHz	0.2 V	50 dB
[6]	9300 mW	900 MHz	15 V	51.6 dB
[7]	240 mW	2.4 GHz	3 V	50 dB
[10]	270 mW	2.4 GHz	1.7 V	73 dB

VI. CONCLUSION

In this effort, we have presented a fully energy autonomous two-way tunnel diode-based repeater node for application in the IoT and WSNs, particularly applicable in scenarios where there is no line of sight between the interrogating reader and tags equipped with sensor information or other data that are of interest. Although there have been ultralong-range RFIDs reported in the literature having read range in excess of 100 m [1], [12], dense implementations of these tag architectures become expensive due to the cost of the active elements in use. The work presented here presents a midrange solution with active elements present at only the repeater nodes of the system, thus enabling increased performance while maintaining low total power consumption. The evaluated system outperforms similar technologies most notably in its ultralow power consumption and operating voltage, as highlighted in Table I. The system was demonstrated capable of extending the range of a semipassive RFID tag by 4.55 times while consuming a mere 40 μ W over 1000 times less than similar technology while maintaining similar performance. This enables it to be powered autonomously and without need for any batteries. The system presents an ideal solution for range and coverage extension of RFIDs in WSNs. Extension of the repeater system to cover arbitrary areas is a promising area of continuing research. The simulation results presented in this article show that even more extreme range coverage with a single repeater node is possible, so cascaded links open up the possibilities for use in a wide variety of applications.

REFERENCES

[1] F. Amato, H. M. Torun, and G. D. Durgin, "RFID backscattering in long-range scenarios," *IEEE Trans. Wireless Commun.*, vol. 17, no. 4, pp. 2718–2725, Apr. 2018.

[2] A. O. Adeyeye, J. Hester, and M. M. Tentzeris, "Miniaturized millimeter wave RFID tag for spatial identification and localization in Internet of Things applications," in *Proc. 49th Eur. Microw. Conf. (EuMC)*, Oct. 2019, pp. 105–108.

[3] C. A. Lynch, A. O. Adeyeye, J. G. D. Hester, and M. M. Tentzeris, "When a single chip becomes the RFID reader: An ultra-low-cost 60 GHz reader and mmID system for ultra-accurate 2D microlocalization," in *Proc. IEEE Int. Conf. RFID (RFID)*, Apr. 2021, pp. 1–8.

[4] J. Kimionis, A. Bletsas, and J. N. Sahalos, "Increased range bistatic scatter radio," *IEEE Trans. Commun.*, vol. 62, no. 3, pp. 1091–1104, Mar. 2014.

[5] A. Varshney and L. Corneo, "Tunnel emitter: Tunnel diode based low-power carrier emitters for backscatter tags," in *Proc. 26th Annu. Int. Conf. Mobile Comput. Netw. (MobiCom)*. New York, NY, USA: Association for Computing Machinery, Sep. 2020, pp. 1–14.

[6] A. G. Dimitriou, "Design, analysis, and performance evaluation of a UHF RFID forward-link repeater," *IEEE J. Radio Freq. Identificat.*, vol. 4, no. 2, pp. 73–82, Jun. 2020.

[7] Y. J. Song and K. Sarabandi, "Miniaturized radio repeater for enhanced wireless connectivity of ad-hoc networks," *IEEE Trans. Antennas Propag.*, vol. 60, no. 8, pp. 3913–3920, Aug. 2012.

[8] S. Sabesan, M. Crisp, R. V. Penty, and I. H. White, "Passive UHF RFID interrogation system using wireless RFID repeater nodes," in *Proc. IEEE Int. Conf. RFID (RFID)*, Apr. 2013, pp. 136–143.

[9] Y. J. Song and K. Sarabandi, "A simultaneous dual-channel micro-radio-repeater for ad-hoc wireless communication," *IEEE Trans. Antennas Propag.*, vol. 62, no. 6, pp. 3378–3383, Jun. 2014.

[10] M. Kashanianfard and K. Sarabandi, "Directional full-duplex RF booster for 2450 MHz ISM band," *IEEE Trans. Antennas Propag.*, vol. 65, no. 1, pp. 134–141, Jan. 2017.

[11] J. Kimionis, M. M. Tentzeris, A. Georgiadis, and A. Collado, "Inkjet-printed reflection amplifier for increased-range backscatter radio," in *Proc. 44th Eur. Microw. Conf.*, Oct. 2014, pp. 5–8.

[12] A. Varshney, A. Soleiman, and T. Voigt, "TunnelScatter: Low power communication for sensor tags using tunnel diodes," in *Proc. 25th Annu. Int. Conf. Mobile Comput. Netw. (MobiCom)*. New York, NY, USA: Association for Computing Machinery, Oct. 2019, pp. 1–17.

[13] A. Eid, J. Hester, and M. M. Tentzeris, "A 5.8 GHz fully-tunnel-diodes-based 20 μ W, 88 mV, and 48 dB-gain fully-passive backscattering RFID tag," in *IEEE MTT-S Int. Microw. Symp. Dig.*, Aug. 2020, pp. 607–610.

[14] A. Adeyeye, C. Lynch, A. Eid, J. Hester, and M. Tentzeris, "5.8-GHz low-power tunnel-diode-based two-way repeater for non-line-of-sight interrogation of RFIDs and wireless sensor networks," *IEEE Microw. Wireless Compon. Lett.*, vol. 31, no. 6, pp. 794–797, Jun. 2021.

[15] H. S. Sommers, "Tunnel diodes as high-frequency devices," *Proc. IRE*, vol. 47, no. 7, pp. 1201–1206, Jul. 1959.

[16] W. Guter and A. Bett, "I-V characterization of tunnel diodes and multijunction solar cells," *IEEE Trans. Electron Devices*, vol. 53, no. 9, pp. 2216–2222, Sep. 2006.

[17] J. G. D. Hester and M. M. Tentzeris, "A mm-wave ultra-long-range energy-autonomous printed RFID-enabled Van-Atta wireless sensor: At the crossroads of 5G and IoT," in *IEEE MTT-S Int. Microw. Symp. Dig.*, Jun. 2017, pp. 1557–1560.



Ajibayo O. Adeyeye (Graduate Student Member, IEEE) received the B.S. degree (*magna cum laude*) in electrical and electronics engineering from the Rose-Hulman Institute of Technology, Terre Haute, IN, USA, in 2017. He is currently pursuing the Ph.D. degree in electrical engineering at the Georgia Institute of Technology, Atlanta, GA, USA.

His research interests lie at the intersection of radar and radio frequency identification (RFID) systems for localization applications.

Mr. Adeyeye received the first place in the 2019 IEEE Microwave Theory and Techniques Society International Microwave Symposium Student Design Competition on Backscatter Radio. He was a Best Student Paper Finalist at the 2021 International Microwave Symposium.



Charles Lynch (Graduate Student Member, IEEE) received the B.S. degree in electrical engineering from the Rose-Hulman Institute of Technology, Terre Haute, IN, USA, in 2019. He is currently pursuing the dual M.S. and Ph.D. degree in electrical engineering at the Georgia Institute of Technology, Atlanta, GA, USA.

He is currently a Research Assistant with the ATHENA Group, Georgia Institute of Technology. His current research interests focus on the design, simulation, and fabrication of radio frequency (RF) and millimeter-wave devices, specifically radio frequency identifications (RFIDs) and millimeter-wave identifications (mmIDs) and combining these low-power, wearable, ultralow-cost devices with radar for the Internet of Things systems.



Aline Eid (Graduate Student Member, IEEE) received the M.S. degree in electrical and computer engineering from the American University of Beirut, Beirut, Lebanon, in 2017, and the Ph.D. degree in electrical and computer engineering from the Georgia Institute of Technology, Atlanta, GA, USA, in 2021.

She is currently a Post-Doctoral Associate at the MIT Media Laboratory, Signal Kinetics Group, Massachusetts Institute of Technology, Cambridge, MA, USA. In 2020, she did a six-month internship with the Google wearable/augmented reality (AR)/virtual reality (VR) and advanced technology & projects (ATAP) groups. She is an inventor of four patents. She has authored or coauthored more than 40 conference papers and journal articles and book chapters. Her research interests are in millimeter-wave (mm-wave)-enabled harvesting and backscattering communications solutions for smart environments and autonomous robots and vehicles.

Dr. Eid was a recipient of the 2020 IEEE MTT-S Graduate Fellowship and Tom Brazil Awards and the First Place Award in the Student Poster Competition at the 2020 FLEX MEMS Sensors Technical Congress. During her master's and Ph.D. studies, she was a recipient of more than 16 awards. At the 2019 IEEE IMS conference, she received the first place in the Radio Frequency Identification (RFID) Student Design Competition, the second place and audience choice in the 3MT Competition, and an Honorable Mention in the Student Paper Competition. She received the first place in the Best Student Paper Award Competition at the 2021 IEEE AP-S.



Jimmy G. D. Hester (Member, IEEE) received the M.S. and Ph.D. degrees in electrical and computer engineering from the Georgia Institute of Technology, Atlanta, GA, USA, in 2014 and 2019, respectively.

He is currently a Co-Founder of Atheraxon, Inc., Atlanta, GA, USA, the company commercializing the 5G radio frequency identification (RFID) technology. He has been developing solutions for the use of carbon nanomaterials as well as optimized radio frequency (RF) structures toward the implementation of inkjet-printed flexible low-cost ubiquitous gas sensors for the Internet of Things and smart skin applications. His work covers the entire development process, from the development of inkjet inks, improvement of fabrication methods, sensor component design, high-frequency characterization and environmental testing to the design, simulation, and fabrication of the RF system embedding the sensor, and the development of wireless reading and data processing schemes. His research interests lie at the interface between RF and millimeter-wave engineering and material science, in the form of flexible electronics technologies and nanotechnologies.

Dr. Hester received the 2015 NT4D Student Award, the Second Place Best Poster Award at the 2017 IEEE Futurecar Conference, the Third Place Best Poster Award at the 2017 Flex Conference, and the Honorable Mention Award as a finalist of the 2017 IMS Student Paper Competition.



Manos M. Tentzeris (Fellow, IEEE) received the Diploma degree (*magna cum laude*) in electrical and computer engineering from the National Technical University of Athens, Athens, Greece, in 1992, and the M.S. and Ph.D. degrees in electrical engineering and computer science from the University of Michigan, Ann Arbor, MI, USA, in 1994 and 1998, respectively.

He was a Visiting Professor with the Technical University of Munich, Munich, Germany, in 2002, GTRI-Ireland, Athlone, Ireland, in 2009, and LAAS-CNRS, Toulouse, France, in 2010. He is currently the Ken Byers Professor of flexible electronics with the School of Electrical and Computer Engineering, Georgia Institute of Technology, Atlanta, GA, USA, where he heads the ATHENA Research Group (20 researchers). He was the Head of the GTECE Electromagnetics Technical Interest Group, an Associate Director of radio frequency identification (RFID)/sensors research at the Georgia Electronic Design Center, an Associate Director of RF Research at the Georgia Institute of Technology NSF-Packaging Research Center, and the RF Alliance Leader. He has authored more than 650 papers in refereed journals and conference proceedings, five books, and 25 book chapters. He has helped develop academic programs in 3-D/inkjet-printed RF electronics and modules, flexible electronics, origami and morphing electromagnetics, highly integrated/multilayer packaging for radio frequency (RF) and wireless applications using ceramic and organic flexible materials, paper-based RFIDs and sensors, wireless sensors and biosensors, wearable electronics, "green" electronics, energy harvesting and wireless power transfer, and nanotechnology applications in RF, microwave MEMS, and system-on-package (SOP)-integrated (UWB, multiband, mmW, and conformal) antennas.

Dr. Tentzeris is a member of the URSI-Commission D and the MTT-15 Committee, an Associate Member of EuMA, a Fellow of the Electromagnetic Academy, and a member of the Technical Chamber of Greece. He served as one of the IEEE MTT-S Distinguished Microwave Lecturers from 2010 to 2012 and is one of the IEEE CRFID Distinguished Lecturers. He was a recipient/co-recipient of the 2019 Humboldt Research Prize, the 2017 Georgia Institute of Technology Outstanding Achievement in Research Program Development Award, the 2016 Bell Labs Award Competition 3rd Prize, the 2015 IET Microwaves, Antennas, and Propagation Premium Award, the 2014 Georgia Institute of Technology ECE Distinguished Faculty Achievement Award, the 2014 IEEE RFID-TA Best Student Paper Award, the 2013 IET Microwaves, Antennas and Propagation Premium Award, the 2012 FiDiPro Award in Finland, the iCMG Architecture Award of Excellence, the 2010 IEEE Antennas and Propagation Society Piergiorgio L. E. Uslenghi Letters Prize Paper Award, the 2011 International Workshop on Structural Health Monitoring Best Student Paper Award, the 2010 Georgia Institute of Technology Senior Faculty Outstanding Undergraduate Research Mentor Award, the 2009 IEEE TRANSACTIONS ON COMPONENTS AND PACKAGING TECHNOLOGIES Best Paper Award, the 2009 E. T. S. Walton Award from the Irish Science Foundation, the 2007 IEEE AP-S Symposium Best Student Paper Award, the 2007 IEEE MTT-S IMS Third Best Student Paper Award, the 2007 ISAP 2007 Poster Presentation Award, the 2006 IEEE MTT-S Outstanding Young Engineer Award, the 2006 Asia-Pacific Microwave Conference Award, the 2004 IEEE TRANSACTIONS ON ADVANCED PACKAGING Commendable Paper Award, the 2003 NASA Godfrey "Art" Anzic Collaborative Distinguished Publication Award, the 2003 IBC International Educator of the Year Award, the 2003 IEEE CPMT Outstanding Young Engineer Award, the 2002 International Conference on Microwave and Millimeter-Wave Technology Best Paper Award, Beijing, China, the 2002 Georgia Institute of Technology—ECE Outstanding Junior Faculty Award, the 2001 ACES Conference Best Paper Award, the 2000 NSF CAREER Award, and the 1997 Best Paper Award of the International Hybrid Microelectronics and Packaging Society. He was the TPC Chair of the IEEE MTT-S IMS 2008 Symposium and the 2005 IEEE CEM-TD Workshop. He is the Vice-Chair of the RF Technical Committee (TC16) of the IEEE CPMT Society. He is the Founder and the Chair of the RFID Technical Committee (TC24) of the IEEE MTT-S and the Secretary/Treasurer of the IEEE C-RFID. He is an Associate Editor of the IEEE TRANSACTIONS ON MICROWAVE THEORY AND TECHNIQUES, the IEEE TRANSACTIONS ON ADVANCED PACKAGING, and the *International Journal on Antennas and Propagation*. He has given more than 100 invited talks to various universities and companies all over the world.